Philippine Journal of Science
150 (1): 201-208, February 2021
ISSN 0031 - 7683
Date Received: 13 Jul 2020

Determination of Dose Distributions by High-energy Electrons in Alumina Pellets Using Monte Carlo Simulations

Frederick C. Hila[1,2]*, **Haydee M. Solomon**[1], **Andrea G. Baule**[1], **Cheri Anne M. Dingle**[1], **Neil Raymund D. Guillermo**[1], and **Rinlee Butch M. Cervera**[3]

[1]Department of Science and Technology – Philippine Nuclear Research Institute
Commonwealth Avenue, Diliman, Quezon City 1101 Metro Manila, Philippines
[2]Materials Science and Engineering Program
[3]Department of Mining, Metallurgical and Materials Engineering
College of Engineering, University of the Philippines
Diliman, Quezon City 1101 Metro Manila, Philippines

Electron beam accelerators are broadly used to study the effects of ionizing radiation on the properties of materials. These accelerators are also used to study radiation effects in some important ceramics such as alumina. The produced high-energy electrons at MeV energies will deposit doses that are typically non-uniformly distributed within the entire material. Such distributions provide valuable information regarding the degree of internal and surface changes owing to the irradiation. In the present study, the Monte Carlo (MC) method was used to obtain the dose distributions of high-energy electrons to alumina ceramic in pellet form. The distributions obtained *via* MCNP5 (Monte Carlo N-Particle version 5) were normalized by experimental values. For the energy of the simulated electrons, both monoenergetic and polyenergetic source electron energies were evaluated. The distributions of the depth-dose, depth-energy, and the top and bottom surface 2D dose mesh were obtained. Results showed that either assumption of monoenergetic or polyenergetic source electron energies resulted in similar depth-dose curves. The depth-energy results showed a larger spread in energy distributions for polyenergetic as compared to monoenergetic source electrons; nonetheless, the average doses for both were similar. The 2D dose maps showed a uniform dose distribution at the top pellet surface and a significantly non-uniform distribution at the bottom of the pellet. These results emphasize the effectiveness of the MC method in determining non-uniform doses within materials, which can be used in quantifying the changes in the material properties at each separate area of the electron irradiated object.

Keywords: aluminum oxide, dose-depth, E-beam, edge effect, energy-depth, MCNP

INTRODUCTION

Electron beam (E-beam) accelerators are widely used in multiple industrial and medical applications and investigations (Zhang *et al.* 2019; Uribe *et al.* 2009; Zeng *et al.* 2005; Marrale *et al.* 2015). E-beams are used in important radiotherapy research, for instance in examining the FLASH effect for efficient tumor treatment (Favaudon *et al.* 2014; Durante *et al.* 2017). E-beams are also largely used in investigating grafting and crosslinking of natural and synthetic polymers, as well as degradation and radiation damage applications (Pomicpic *et al.* 2020; Madrid *et al.* 2017; Kusumoto *et al.* 2016, 2020a). More

*Corresponding Author: fchila@pnri.dost.gov.ph

than 1500 of these accelerators are used worldwide in radiation processing (IAEA 2010).

Such accelerators are also used for radiation damage studies to ceramics (Bonevich and Marks 1991; Hobbs 1979; Jiang 2015) that are important in fields where ionizing environments are present (Thomé *et al.* 2012). Some ceramics have been shown to display various phenomenon upon electron irradiation, inducing changes in grain sizes (Huang *et al.* 2015; Surzhikov *et al.* 2015), fast crystallizations (Huang *et al.* 2015), structural growths, and formation of nanoparticles (Longo *et al.* 2013; Sczancoski *et al.* 2019). One of the most abundant ceramics present in the Earth's crust is aluminum oxide (Al_2O_3) or alumina. The alumina ceramic is used in aerospace and nuclear industries for applications in high-energy radiations because of its excellent physical, chemical, and thermal properties (Richards 1991; Tang and Yu 2015; Visakh *et al.* 2017).

Important changes have been demonstrated by E-beam irradiation of alumina. These include grain modifications, phase transformations, and crystallizations (Othman *et al.* 2015; Nakamura *et al.* 2013; Jasim *et al.* 2019; Hila *et al.* 2020). For sapphire crystals (that is the single crystal form of α-alumina), irradiations have also been employed for ion (titanium and chromium) diffusion in altering color varieties (Ahn *et al.* 2009, 2011, 2013). Moreover, alumina is used in radiation dosimeter applications (De Barros *et al.* 2007; Magne *et al.* 2008) and is now used as passive nuclear track detectors aimed at neutron, proton, and charged ion dosimetry (Akselrod *et al.* 2003; Akselrod and Kouwenberg 2018; Kodaira *et al.* 2020; Kusumoto *et al.* 2020b). Therefore, irradiation research of the alumina is important for various applications of this ceramic material. This includes studying the morphological changes in the material as a function of the dose or energy of the specific radiation (Othman *et al.* 2015; Nakamura *et al.* 2013).

In characterizing the morphological changes in irradiated objects, it is common to report the doses received as well as the source radiation type and energy. The most important quantity in the irradiation of a medium with ionizing radiation is the absorbed dose. Nonetheless, few morphological characterization studies have focused on obtaining dose distributions within and at the surfaces of the material. For charged particle irradiation, acquisition of such dose distributions presents a useful opportunity since a single target object can receive a variety of doses (IAEA 2010). Therefore, the irradiation of the object under an E-beam can be used for the study of morphological effects at varying doses using only a single homogenized sample. Since the absorbed dose is commonly related to changes within a material, dose distributions can be very useful in morphological investigations of irradiation effects.

In the present study, we attempt to evaluate the dose distributions of an E-beam into alumina ceramics in pellet form. To acquire dose distributions within an irradiated object, the most desirable method is *via* MC simulations (IAEA 2010) since it accounts for the geometry of the sample as well as the entire irradiation environment (Mittendorfer and Niederreiter 2020). This method is generally used to obtain depth-dose curves of high-energy electrons to water phantoms for radiotherapy (Kesen *et al.* 2014; Park *et al.* 2016, 2018; Sardari *et al.* 2010), but has also been used to determine doses for E-beams incident on aluminum wedges, radiation dosimeters, and can also be extended for industrial products (Mittendorfer and Niederreiter 2020; Vandana *et al.* 2018; Matsui *et al.* 2018; IAEA 2010). Computer codes typically used are MCNP, Geant4, and PENELOPE (Sempau *et al.* 2001; Batic *et al.* 2013; Peri and Orion 2017).

The goal of this investigation is to show the viability, convenience, and usefulness of the MC method in determining the non-uniform dose distribution of E-beams within the entire material. This method could prove useful in quantifying the changes in material properties at different parts or surfaces of the object. The MCNP5 code was used for the simulation of high-energy electrons incident onto the alumina pellet while considering the environment geometry. Distributions obtained *via* the MC method were normalized to absorbed doses obtained experimentally using dosimetric films. The distributions obtained in this work include the central axis depth-dose and depth-energy, the depth-dose for double-sided irradiation, and 2D surface dose maps of both the top and bottom surfaces of the pellet.

MATERIALS AND METHODS

Experiments

The alumina pellet was synthesized in this work using a sol-gel method described in our previous study (Hila *et al.* 2020). The synthesized powder was pressed at 2 tons with a 13-mm diameter and was subsequently heated at 1100 °C. After synthesis, the 1.3-mm thick pellet was sent to the E-beam accelerator facility of the Philippine Nuclear Research Institute.

The pellet was irradiated using 2-MeV electrons at an approximate dose of 50 kGy. During irradiation, the pellet was encased in a Petri dish container with a top covering. The energy of the E-beam was calibrated using an aluminum wedge (ISO/ASTM 51649).

The approximate dose was determined by the average of the top and bottom readings of the alumina pellet. These

were experimentally obtained by placing dosimetric films (GEX B3 Windose USA) at these surfaces. The films were subsequently analyzed using a Shimadzu UVMini-1240 UV-Vis spectrophotometer.

MC Simulations

The MCNP5 code is a multi-purpose radiation transport software package for coupled electron, photon, and neutron simulations (X-5 Monte Carlo Team 2008). This was used to obtain the E-beam dose distributions inside and at the surface of the alumina pellet. The geometries external to the pellet were modeled, as shown in Figure 1. A parallel beam of electrons was generated through a modeled disk source. Furthermore, the electron minimum energy cut-off was set to 100 keV to serve to reduce the variance.

For electron energies, two assumptions were individually considered: a) monoenergetic beam of electrons at 2 MeV only, and b) polyenergetic beam with Gaussian distribution of 2.0 ± 0.2 MeV (or 2 MeV with a 10% relative standard deviation). The latter is a practical approximation since the energy of electrons from E-beams typically have large spreads (IAEA 2010).

To obtain simulation results, the pellet was modeled using two different geometries shown in Figures 2a and 2b. The first (Figure 2a) pellet model was used to obtain absorbed dose and electron energy as a function of depth, whereas the latter (Figure 2b) model was used to obtain the surface 2D absorbed dose mesh of the pellet. In both geometries, the single pellet was sliced into multiple cells. For the first pellet model (Figure 2a), a total of 100 layers were implemented. For the second pellet model (Figure 2b), both surface mesh models were 100 μm thick with 100 radial slices.

For obtaining electron energies as a function of depth, the F2 tally with energy card was used on the top surfaces of each cell in Figure 2a. On the other hand, to obtain absorbed doses, the cells in both models Figures 2a and 2b were declared as detectors with *F8 tally for energy deposition within each cell. The results of each tally were divided by the corresponding cell mass.

All simulations were carried out using a desktop computer with processor Intel® Core™ i7-6700 CPU @ 3.4 GHz. For each simulation, a total of 10 billion starting electron particles were generated to achieve negligible relative errors.

RESULTS AND DISCUSSION

Depth-Dose and Depth-Energy Plots

Experimental irradiation of the pellet was accomplished at an average absorbed dose of 53 kGy. This was the average of the top and bottom film dosimeter measurements for the

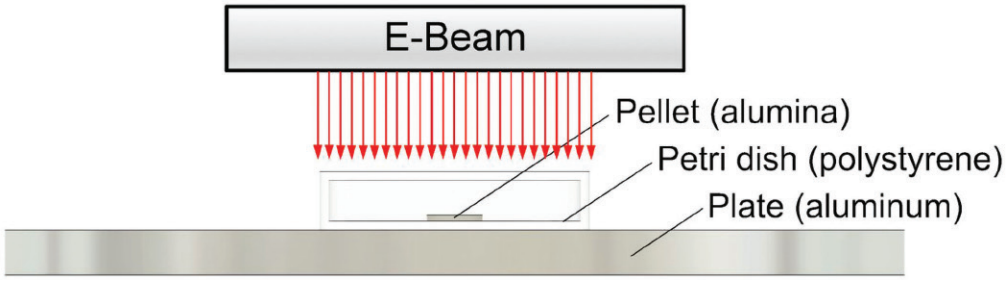

Figure 1. Geometry setup of MC simulations.

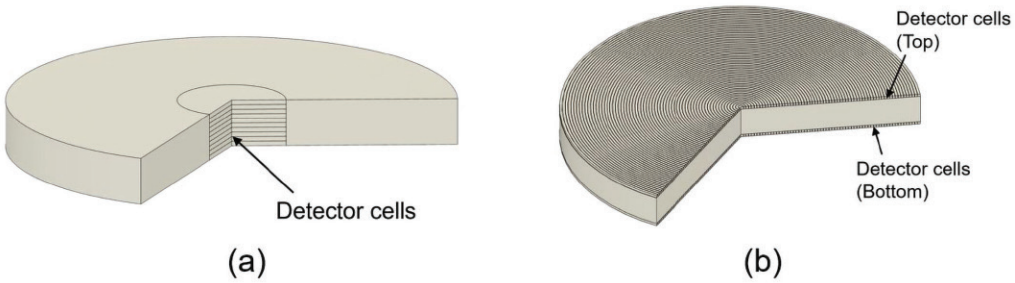

Figure 2. Geometries of alumina pellet for MC simulations of (a) central axis depth-dose and depth-energy plots, and (b) 2D dose mesh.

alumina pellet. The top film measurement was at 45 ± 2 kGy and the bottom film measurement was at 62 ± 3 kGy.

For the central axis depth-dose curve of the pellet, the simulation results from MCNP5 are shown in Figure 3a, in units of absorbed dose per source electron. There is little difference between the curve produced by a monoenergetic beam and by a Gaussian energy distributed beam. This is consistent with others for high-energy electron beams but the incident on water samples (Haryanto 2010; Park *et al.* 2018). Figure 3b shows both curves normalized to the experimental measurements. An excellent fit was achieved, likely because of the inclusion of the most significant environment geometries such as the Petri dish container, aluminum platform, and air atmosphere.

Moreover, the figures show that at the location of maximum dose, there is a 40% higher value relative to the minimum dose location which is the top surface. Starting from the top and downwards, the dose is initially increasing with depth. This is mainly due to the energy deposition of cascading secondary electrons and reduction in electron energies leading to increased collision stopping power that relates to the increase in deposited energy per unit distance. The slight downtrend near the bottom surface also suggests that as the pellet thickness increases further, the bottom dose measurements begin to decrease. Although expected, it is significant to establish since absorbed doses are typically reported as the average of top and bottom film readings. Therefore, underestimations of the doses at the innards of such pellets are likely to be made.

The effect of double-sided irradiation to produce a symmetric depth-dose distribution of the pellet is shown in Figure 3c. This denotes the use of two irradiation passes into the E-beam accelerator, wherein in the second pass the pellet is flipped upside down. The symmetric curve will only have a 10% higher dose at the center as compared to both the top and bottom surfaces.

Results of depth-energy plots are shown in Figures 4 and 5 for monoenergetic and Gaussian energy distributed source electrons, respectively. These figures show the degree of energy drop as the electrons pass through the pellet. At the top surface, the average electron energies were slightly below the starting electron energy of 2 MeV. This is mostly

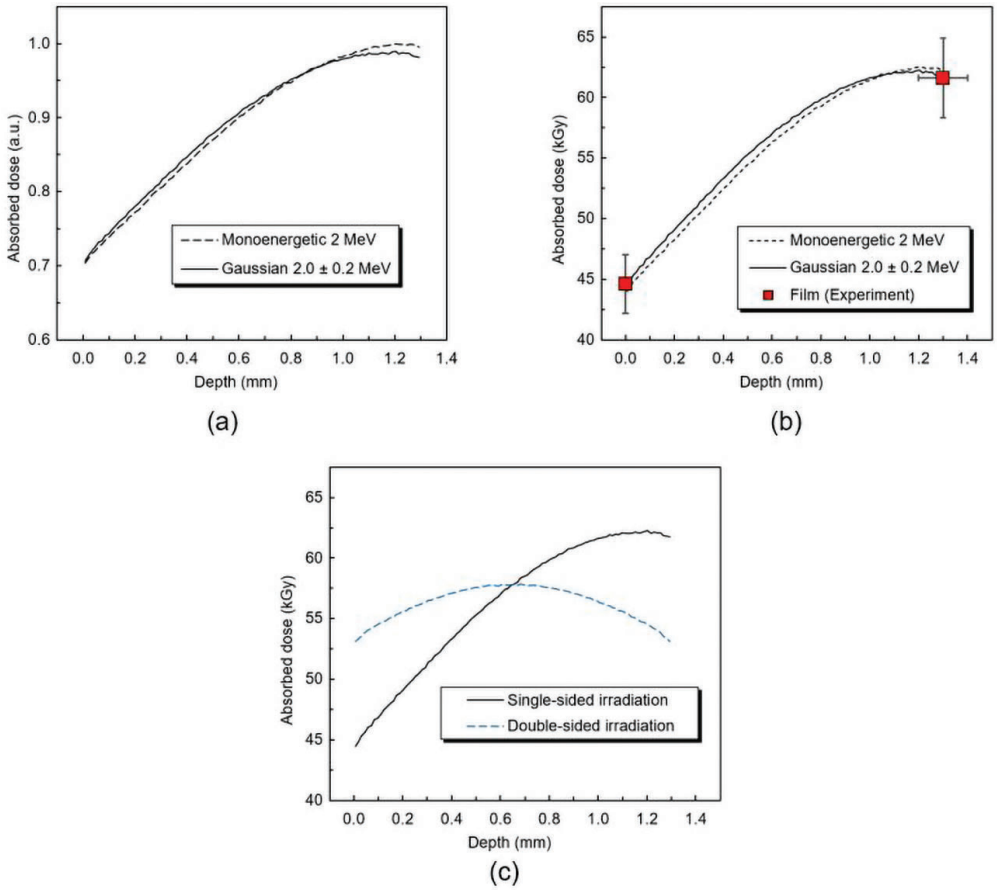

Figure 3. Depth-dose curve of high-energy electrons in an alumina pellet (a) per source electron generated, (b) normalized to experimental dose measurements, and (c) effect of double-sided irradiation.

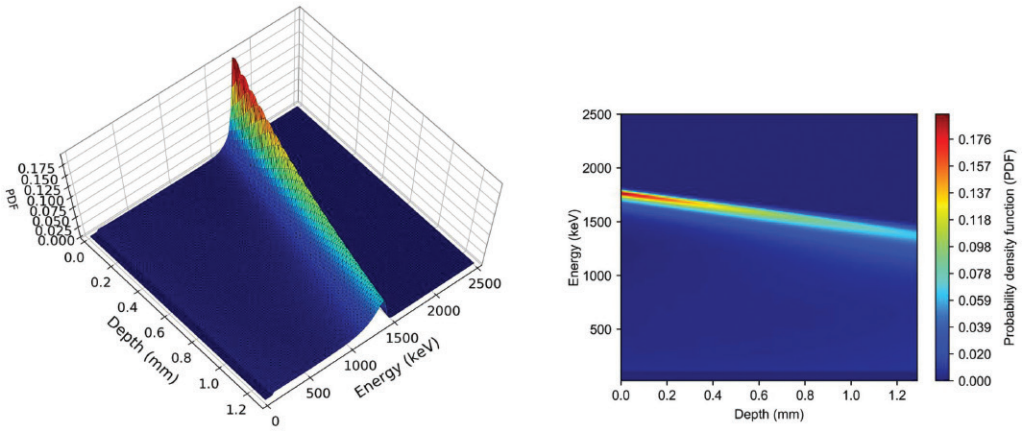

Figure 4. Electron depth-energy plots by monoenergetic source electrons.

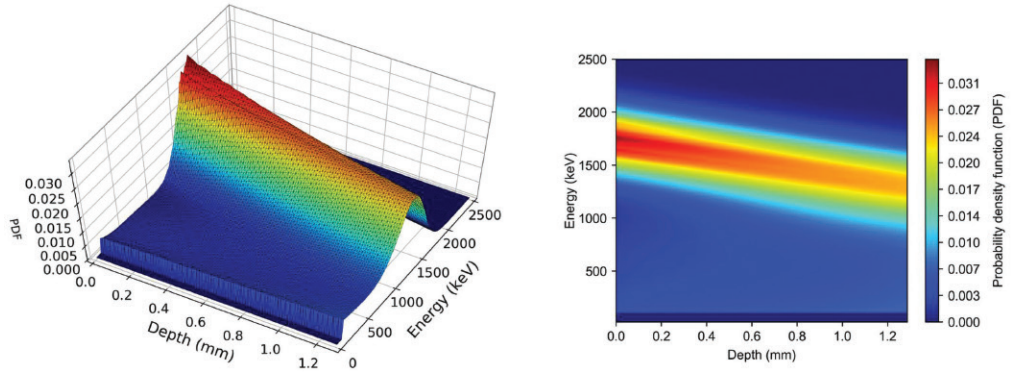

Figure 5. Electron depth-energy plots by Gaussian energy distributed source electrons.

due to the Petri dish cover, which attenuates the electrons before they reach the pellet. This suggests that the Petri dish cover also acts to increase the average absorbed doses received by the pellet, as shown in the initial upward trend beginning at the top surface shown in Figures 3a and 3b.

Moreover, the increasing spread in electron energies as a function of depth is noticeable. A low-energy tail is found for both cases. Nevertheless, in both cases, the average electron energy as a function of depth was found to be similar.

The depth-dose and depth-energy plots translate to different degrees of changes in the material within the entire pellet depth since both absorbed doses and electron energies varied with depth. This is significant as the irradiation-induced changes in this material, including grain size alteration (Othman *et al.* 2015) and atomic rearrangements (Nakamura *et al.* 2013, Jasim *et al.* 2019), are dependent on both absorbed doses and the energy of the incident electrons.

2D Dose Mesh

The results of the 2D dose mesh of the alumina pellet are shown in Figures 6 and 7 for the top and bottom surfaces, respectively. These were obtained using the previous Gaussian energy assumption with dose values normalized to experiment. For the top surface, it is seen that a uniform dose is produced. Therefore, the top surface can serve as a uniform area for the surface characterization of the irradiated alumina, whereas the bottom surface has a significantly non-uniform dose distribution with a higher dose portion at the center. This edge effect (IAEA 2010) could have the potential in studying surface properties at multiple irradiation doses. It is especially useful for morphology data *via* scanning electron microscopes or atomic force microscopy methods using a single homogeneous pellet.

CONCLUSION

The dose distribution of E-beams into alumina ceramic pellets was obtained using MC simulations. The MCNP5 code was used to obtain central axis depth-dose and depth-energy plots and the 2D dose mesh of the pellet. Two energy distributions of the source electrons were assumed: a) monoenergetic 2 MeV electrons and b) Gaussian energy distributed electrons. Results show that both assumptions

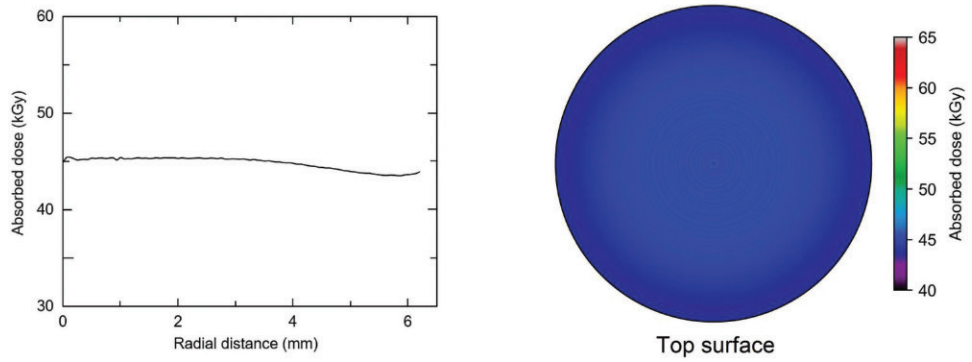

Figure 6. The pellet top surface 2D absorbed dose mesh by Gaussian electron energy distribution.

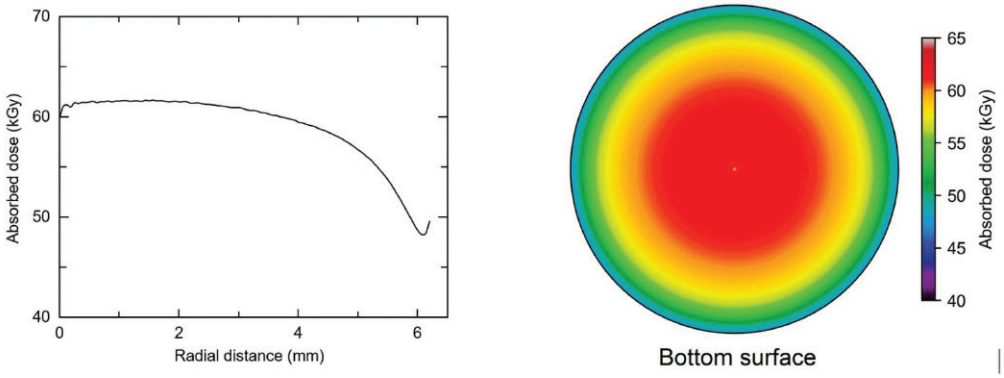

Figure 7. The pellet bottom surface 2D absorbed dose mesh by Gaussian electron energy distribution.

produced no significant difference between absorbed dose curves. Furthermore, the average electron energies as a function of depth were similar in both assumptions. On the other hand, the result of the 2D mesh shows a uniform dose distribution at the top surface and a non-uniform at the bottom surface with a dose drop in the edges of the pellet.

The significance of MC calculations for E-beam irradiation was shown since, unlike high-energy photon irradiation, the use of high-energy charged particle radiation typically results in uneven dose distributions within the products. This is owing to the much less penetrating nature of charged particles that can interact by coulombic forces. The dose distributions can be of significance in quantifying the changes in the material properties brought about by electron irradiation. For instance, radiation degradation studies would be most pronounced at the central bottom part of a similar pellet at similar irradiation conditions. On the other hand, these results also show that the surface morphology of a single pellet can be used to study the effects of irradiation at varying absorbed doses.

REFERENCES

AHN Y-K, SEO J-G, PARK J-W. 2009. Diffusion of chromium in chrysoberyl. J Cryst Growth 311(15): 3943–3947.

AHN Y-K, SEO J-G, PARK J-W. 2011. Diffusion of chromium in sapphire: the effects of electron beam irradiation. J Cryst Growth 326(1): 45–49.

AHN Y, SEO J, WATHANAKUL P, PARK J. 2013. Effects of electron-beam irradiation, a thin-Ti layer, and a BeO additive on the diffusion of titanium in synthetic sapphire. Ceram Int 39(3): 2259–2265.

AKSELROD MS, AKSELROD AE, ORLOV SS, SANYAL S, UNDERWOOD TH. 2003. Fluorescent Aluminum Oxide Crystals for Volumetric Optical Data Storage and Imaging Applications. J Fluoresc 13(6): 503–511.

AKSELROD M, KOUWENBERG J. 2018. Fluorescent nuclear track detectors – review of past, present and future of the technology. Radiat Meas 117: 35–51.

BATIC M, HOFF G, PIA MG, SARACCO P, WEIDENSPOINTNER G. 2013. Validation of Geant4 Simulation of Electron Energy Deposition. IEEE Trans Nucl Sci 60(4): 2934–2957.

BONEVICH JE, MARKS LD. 1991. Electron Radiation Damage of α-alumina. Ultramicroscopy 35: 161–166.

DE BARROS VS, KHOURY HJ, AZEVEDO WM, DA SILVA EF. 2007. Characterization of Nanoporous Al_2O_3:C for Thermoluminescent Radiation Dosimetry. Nucl Instrum Methods Phys Res, Sect A 580: 180–182.

DURANTE M, BRAUER-KRISCH E, HILL M. 2017. Faster and safer? FLASH ultra-high dose rate in radiotherapy. Br J Radiol 20170628.

FAVAUDON V, CAPLIER L, MONCEAU V, POUZOULET F, SAYARATH M, FOUILLADE C, POUPON MF, BRITO I, HUPÉ P, BOURHIS J, HALL J, FONTAINE JJ, VOZENIN MC. 2014. Ultrahigh dose-rate FLASH irradiation increases the differential response between normal and tumor tissue in mice. Sci Transl Med 6(245): 245ra93–245ra93.

HARYANTO F. 2010. Study on the effect of energy parameter of electron on the percentage depth dose of electron beam using Monte Carlo method. AIP Conf Proc 1244(2010): 168–172.

HILA F, PAYOT AJ, RALLOS R, GUILLERMO NR, CERVERA RB. 2020. Morphology of alumina particles synthesized by sol-gel method and irradiated with high-energy electrons. Proceedings of the Samahang Pisika ng Pilipinas 38: SPP-2020-PA-01.

HOBBS LW. 1979. Application of Transmission Electron Microscopy to Radiation Damage in Ceramics. J Am Ceram Soc 62(5–6): 267–278.

HUANG Z, QI J, ZHOU L, FENG Z, YU X, GONG Y, YANG M, SHI Q, WEI N, LU T. 2015. Fast crystallization of amorphous $Gd_2Zr_2O_7$ induced by thermally activated electron-beam irradiation. J Appl Phys 118(21).

[IAEA] International Atomic Energy Agency. 2010. Use of Mathematical Modelling in Electron Beam Processing: A Guidebook. IAEA Radiation Technology Series No. 1.

ISO/ASTM-51649. 2005. Standard Practice for Dosimetry in Electron Beam Facility Radiation Processing at Energy between 300 keV and 20 MeV. ISO/ASTM International, West Conshohocken, PA.

JASIM A, HE X, WHITE T, XING Y. 2019. Crystallization of Amorphous Alumina Whiskers on Carbon Nanotubes Under Electron Beam Irradiation. Microsc Microanal 25(Suppl 2): 1988–1989.

JIANG N. 2015. Electron beam damage in oxides: a review. Rep Prog Phys 79(1): 16501.

KESEN ND, CAKIR A, OKUTAN M, BILGE H. 2014. Research of dosimetry parameters in small electron beams. Sci Technol Nucl Install 2014: 1–7.

KODAIRA S, KUSUMOTO T, KITAMURA H, YANAGIDA Y, KOGUCHI Y. 2020. Characteristics of fluorescent nuclear track detection with Ag^+-activated phosphate glass. Radiat Meas 132: 106252.

KUSUMOTO T, MORI Y, KANASAKI M, ODA K, KODAIRA S, HONDA Y, TOJO S, BARILLON R, YAMAUCHI T. 2016. Sudden Increase of the Radiation Chemical Yield for Loss of Carbonate Ester in PADC Detector where the Track Overlapping of 28 MeV Electrons Becomes Significant. Proceedings of International Symposium on Radiation Detectors and Their Uses (ISRD2016). Proceedings of International Symposium on Radiation Detectors and Their Uses (ISRD2016).

KUSUMOTO T, OKADA S, KURASHIGE H, KOBAYASHI K, FROMM M, RAFFY Q, LUDWIG N, KANASAKI M, ODA K, HONDA Y, TOJO S, GROETZ JE, OGAWARA R, KODAIRA S, BARILLON R, YAMAUCHI T. 2020a. Evidence for a critical dose above which damage to carbonate ester bonds in PADC appear after gamma ray and ultra soft X-ray exposures. Radiat Phys Chem 170: 108628.

KUSUMOTO T, MATSUYA Y, BABA K, OGAWARA R, AKSELROD MS, HARRISON J, FOMENKO V, KAI T, ISHIKAWA M, HASEGAWA S, KODAIRA S. 2020b. Verification of dose estimation of Auger electrons emitted from Cu-64 using a combination of FNTD measurements and Monte Carlo simulations. Radiat Meas 132: 106256.

LONGO E, CAVALCANTE LS, VOLANTI DP, GOUVEIA AF, LONGO VM, VARELA JA, ORLANDI MO, ANDRÉS J. 2013. Direct *in situ* observation of the electron-driven synthesis of Ag filaments on α-Ag_2WO_4 crystals. Sci Rep 3: 4–7.

MADRID JF, CABALAR PJE, ABAD LV. 2017. Radiation-induced graft polymerization of acrylic acid and glycidyl methacrylate onto abaca/polyester nonwoven fabric. J Nat Fibers 15(5): 625–638.

MAGNE S, AUGER L, BORDY JM, DE CARLAN L, ISAMBERT A, BRIDIER A, FERDINAND P, BARTHE J. 2008. Multichannel Dosemeter and Al_2O_3:C Optically Stimulated Luminescence Fibre Sensors for use in Radiation Therapy: Evaluation with Electron Beams. Radiat Phys Chem 131(1): 93–99.

MARRALE M, LONGO A, RUSSO G, CASARINO C, CANDIANO G, GALLO S, CARLINO A, BRAI M. 2015. Dosimetry for electron Intra-operative radiotherapy: comparison of output factors obtained through alanine/EPR pellets, ionization chamber and Monte Carlo-GEANT4 simulations for IORT mobile dedicate accelerator. Nucl Instrum Methods Phys Res Sect B: 358: 52–58.

MATSUI S, HATTORI T, NONAKA T, WATANABE Y, MORITA I, KONDO J, ISHIKAWA M, MORI Y. 2018. Measurement of Relative Depth-Dose Distribution in Radiochromic Film Dosimeters Irradiated with 43–70 keV Electron Beam for Industrial Application. Radiat Phys Chem 146: 91–95.

MITTENDORFER J, NIEDERREITER M. 2020. Intrinsic dose characteristics in electron beam irradiation. Radiat Phys Chem: 109124.

NAKAMURA R, ISHIMARU M, YASUDA H, NAKAJIMA H. 2013. Atomic Rearrangements in Amorphous Al_2O_3 Under Electron-Beam Irradiation. J Appl Phys 113(064312).

OTHMAN NEF, ABDULLAH Y, PURWANTO H, ZAINI KH. 2015. Effect of Electron Beam Irradiation on the Morphology of Alumina Ceramic. Adv Mater Res 1115: 142–145.

PARK H, CHOI HJ, KIM J-I, MIN CH. 2018. Analysis of Dose Distribution According to the Initial Electron Beam of the Linear Accelerator: A Monte Carlo Study. J Radiat Prot Res 43(1): 10–19.

PARK JI, HA SW, KIM J-I, LEE H, LEE J, KIM IH, YE S-J. 2016. Design and evaluation of electron beam energy degraders for breast boost irradiation. Radiat Oncol 11(1): 1–10.

PERI E, ORION I. 2017. Shielding Calculations for Industrial 5/7.5MeV Electron Accelerators Using the MCNP Monte Carlo Code. EPJ Web of Conferences 153(03011): 3–8.

POMICPIC J, DANCEL GC, CABALAR PJ, MADRID J. 2020. Methylene blue removal by poly(acrylic acid)-grafted pineapple leaf fiber/polyester nonwoven fabric adsorbent and its comparison with removal by gamma or electron beam irradiation. Radiat Phys Chem 172: 108737.

RICHARDS G. 1991. Aluminum Oxide Ceramics. Concise Encyclopedia of Advanced Ceramic Materials. p. 16–20.

SARDARI D, MALEKI R, SAMAVAT H, ESMAEELI A. 2010. Measurement of depth-dose of linear accelerator and simulation by use of Geant4 computer code. Rep Pract Oncol Radiother 15(3): 64–68.

SCZANCOSKI JC, MAYA-JOHSON S, DA SILVA PEREIRA W, LONGO E, LEITE ER. 2019. Atomic Diffusion Induced by Electron-Beam Irradiation: An *In Situ* Study of Ag Structures Grown from α-Ag_2WO_4. Cryst Growth Des 19(1): 106–115.

SEMPAU J, SANCHEZ-REYES A, SALVAT F, OULAD BEN TAHAR H, JIANG SB, FERNANDEZ-VAREA JM. 2001. Monte Carlo Simulation of Electron Beams from an Accelerator Head Using PENELOPE. Phys Med Biol 46: 1163–1186.

SURZHIKOV AP, FRANGULYAN TS, GHYNGAZOV SA, VASILIEV IP. 2014. Electron microscopy studies of near-surface layers of ZrO_2(Y)-Al_2O_3 composite ceramic modified by high-current beam of low-energy electrons. Inorg Mater Appl Res 5(5): 536–539.

TANG X, YU Y. 2015. Electrospinning Preparation and Characterization of Alumina Nanofibers with High Aspect Ratio. Ceram Int 41: 9232–9238.

THOMÉ L, MOLL S, DEBELLE A, GARRIDO F, SATTONNAY G, JAGIELSKI J. 2012. Radiation effects in nuclear ceramics. Adv Mater Sci Eng 2012.

URIBE RM, SALVAT F, CLELAND MR, BEREJKA A, MCDANIEL FD, DOYLE BL. 2009. Monte Carlo Simulation of the Irradiation of Alanine Coated Film Dosimeters with Accelerated Electrons. AIP Conference Proceedings. Application of Accelerators in Research and Industry: Twentieth International Conference.

VANDANA S, BENNY PG, SELVAM TP. 2018. Comparison of measured and Monte Carlo-calculated electron depth dose distributions in aluminium. Indian J Pure Appl Phys 56(1): 48–52.

VISAKH PM, NAZARENKO OB, SARATH CHANDRAN C, MELNIKOVA TV, NAZARENKO SY, KIM JC. 2017. Effect of Electron Beam Irradiation on Thermal and Mechanical Properties of Aluminum Based Epoxy Composites. Radiat Phys Chem 136: 17–22.

X-5 MONTE CARLO TEAM. 2008. MCNP – Version 5, Vol. I: Overview and Theory.

ZHANG C, ZHANG M, WU G, WANG Y, ZHANG L. 2019. Radiation Cross-Linking and Its Application. In: Radiation Technology for Advanced Materials. Elsevier. p. 75–113.

ZENG GG, MCEWEN MR, ROGERS DWO, KLASSEN NV. 2005. An experimental and Monte Carlo investigation of the energy dependence of alanine/EPR dosimetry: II. clinical electron beams. Phys Med Biol 50(6): 1119–1129.